On-Demand Maneuvering of Diverse Prodrug Liquids on a Light-Responsive Candle-Soot-Hybridized Lubricant-Infused Slippery Surface for Highly Effective Toxicity Screening

Shuneng Zhou, Chao Chen, Junfeng Yang, Lirui Liao, Zekun Wang, Dong Wu, Jiaru Chu, Li Wen,* and Weiping Ding*

Cite This: *ACS Appl. Mater. Interfaces* 2022, 14, 31667−31676

Read Online

ACCESS | Metrics & More | Article Recommendations | SI Supporting Information

ABSTRACT: At present, microscale high-throughput screening (HTS) for drug toxicity has drawn increased attention. Reported methods are often constrained by the inability to execute rapid fusion over diverse droplets or the inflexibility of relying on rigid customized templates. Herein, a light-responsive candle-soot-hybridized lubricant-infused slippery surface (CS-LISS) was reported by one-step femtosecond laser cross-scanning to realize highly effective and flexible drug HTS. Due to its low-hysteresis merits, the CS-LISS can readily steer diverse droplets toward arbitrary directions at a velocity over 1.0 mm/s with the help of tracing lateral near-infrared irradiation; additionally, it has the capability of self-cleaning and self-deicing. Significantly, by integrating the CS-LISS with a GFP HeLa cell chip, high-efficiency drug toxicity screening can be successfully achieved with the aid of fluorescence imaging. This work provides insights into the design of microscale high-throughput drug screening.

KEYWORDS: *light-responsive slippery surface, candle-soot nanoparticles, micro-droplets, self-cleaning, high-throughput drug screening*
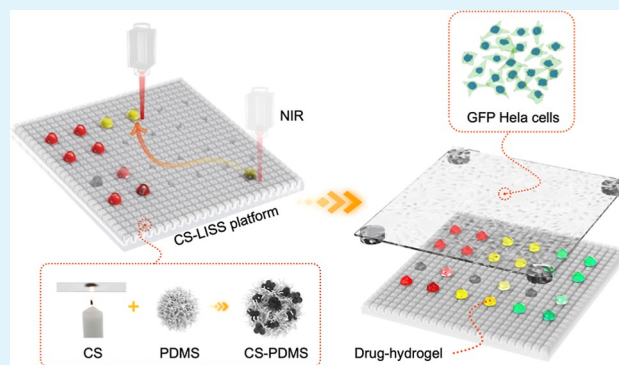
INTRODUCTION

High-throughput screening (HTS) toxicity assays are essential to assess the toxicity of drug candidates early in the discovery process to reduce the chances of later failure.[1] With the development of combinatorial chemistry, genomics, and proteomics, there has been a dramatic increase in the number of screenable drug targets.[2] In recent years, considering that the conventional HTS method using 96- or 384-well plates suffers from several limitations, including inefficient pipetting operations and the difficulty of subsequent washing the cell monolayers,[3−5] microscale HTS is emerging as a hotspot owing to its efficient drug screening and cost-saving merits.[6−9] Accordingly, ink-jet printing,[10−12] superhydrophobic−hydrophilic micropatterns,[13−15] and microfluidics[16] have been explored to produce cell/drug-hydrogel microarrays for HTS. However, the application of these platforms is severely constrained by operational limitations. For example, the fusion of two solutions by printing or superhydrophobic−hydrophilic micropatterns relies on multiple jetting feeds of a pipette to the same point or a chip covering another chip, which is unable to execute complex fusion operations. The former pipetting is cumbersome and inefficient due to the repetitive jet replacement, while the latter chip stack has alignment problems between two chips, where a slight deviation may

cause serious contamination of the drugs. In addition, although microfluidics can realize the fusion operation of various solutions, the templates need to be customized for different hybrid schemes.

Recently, microdroplets have exhibited broad prospects in chemical reactions, medical diagnosis, and biological analysis.[17−21] Today, various methods have been developed for maneuvering droplets, including electric,[22] acoustic,[23] magnetic,[24] wettability gradient,[25] and light-responsive[26−28] methods. Among these methods, by taking advantage of remote, contactless, and low-contact-angle hysteresis features, a light-responsive slippery surface shows superiority in intelligence and controllability and has the potential to be a drug manipulation platform for HTS. For the light-responsive slippery surface, the photothermal dopant plays a vital role as it can induce the generation of asymmetric temperature-difference-caused wetting gradient forces on both sides of the
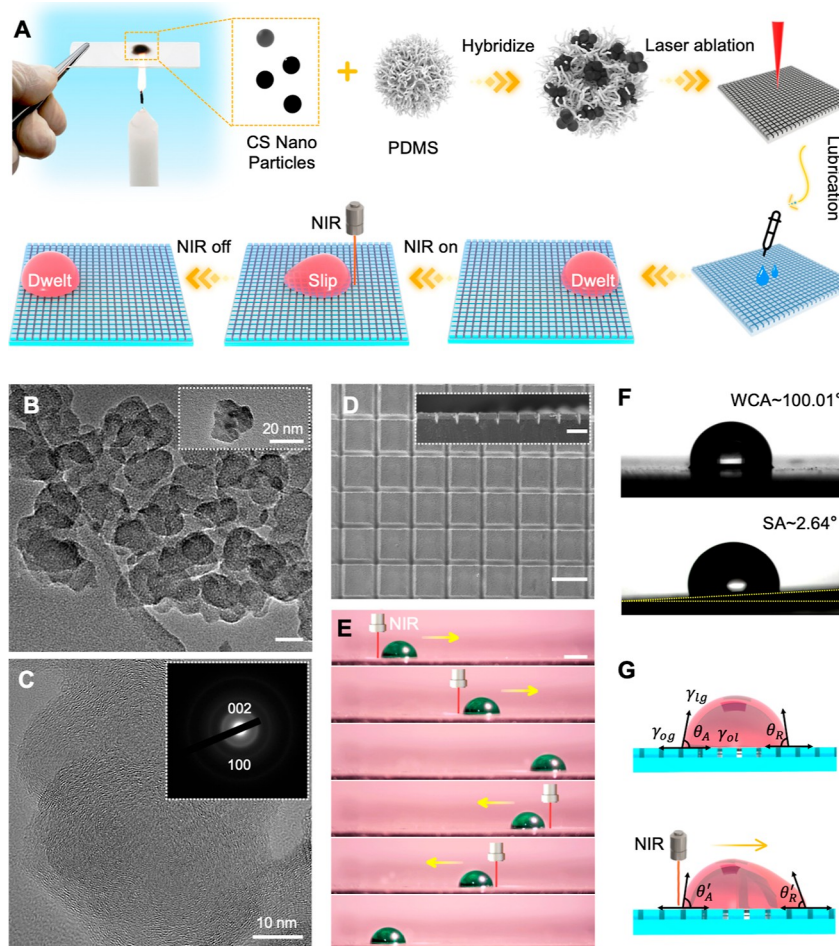
Figure 1. Fabrication of the light-triggered CS-LISS. (A) Schematic of the fabrication of the CS-LISS and manipulation of droplet sliding on the CS-LISS via NIR. (B) FETEM images of CS clusters (scale bar = 20 μm). (C) HRTEM image of CS lusters, and insets show the SAED pattern of CS. (D) SEM images of the top and sectional views of the CS-PDMS film (scale bar = 50 μm). (E) Sliding progress of a droplet on the CS-LISS under NIR irradiation (scale bar = 3 mm). (F) Contact angle and slide angle of water droplets on the CS-LISS. (G) Mechanism illustration of the wettability gradient variation with unilateral NIR irradiation.

manipulated droplets on a lubricated surface after absorbing light energy.[29,30] However, it is challenging to obtain an ideal photothermal dopant for lubricant-infused slippery surfaces (LISSs) that is cheap, easily fabricated, and highly photothermally efficient. Current photothermal dopant materials, such as Fe_3O_4, TiO_2, and graphene, are usually costly and difficult to fabricate, involving sophisticated chemical syntheses and deposition technologies.[31−33] Very recently, candle soot (CS) has received much attention due to its structure and physical properties.[34−36] CS nanoparticles are the incomplete burning products of a candle. It is a type of nanoscale carbon cluster and can form a nearly perfect hierarchical structure, resulting in the superhydrophobicity of CS itself;[37] thus, it is possible to maintain excellent surface hydrophobicity after mixing CS nanoparticles with the host matrix. In addition, CS nanoparticles have an excellent light-to-heat conversion effect[38] and are cheap and easy to acquire. Therefore, it has great potential as a photothermal dopant for light-responsive slippery surfaces.

Herein, in this paper, we propose a light-responsive candle-soot-hybridized lubricant-infused slippery surface (CS-LISS) textured with a one-step femtosecond laser for realizing highly effective and flexible HTS. The CS-LISS platform could readily steer diverse prodrug drops toward arbitrary directions with the help of near-infrared irradiation (NIR): once tracing lateral NIR is loaded, a wettability gradient force is generated for actuating droplets to slide toward intentional orientations. On the CS-LISS, we could realize rapid sorting, patterning, and fusion of prodrug drops at a velocity over 1.0 mm/s. Moreover, the CS-LISS is easily deiced after cryopreservation, enabling it to effectively clear the residual prodrug liquid and then be reused. Significantly, we demonstrated the CS-LISS as a high-throughput drug toxicity screening platform and achieved the rapid generation of prodrug microarrays and fast fusion of multiple prodrugs. Specifically, after the prodrug droplet-laden CS-LISS was combined with a green fluorescence protein (GFP)-stained HeLa cell chip, the effects of drug type/concentration on cells could be distinguished at a high efficiency with fluorescence images, and thereby, high-throughput drug toxicity screening was successfully achieved. This work proposes a light-responsive CS-hybridized lubricant-infused slippery surface and may provide insights for the further development of HTS.

RESULTS AND DISCUSSION

Fabrication of the CS-LISS. The fabrication strategy of the CS-LISS is shown in Figure 1A. CS was collected on a silica glass slide over a candle flame. The structure of the CS is
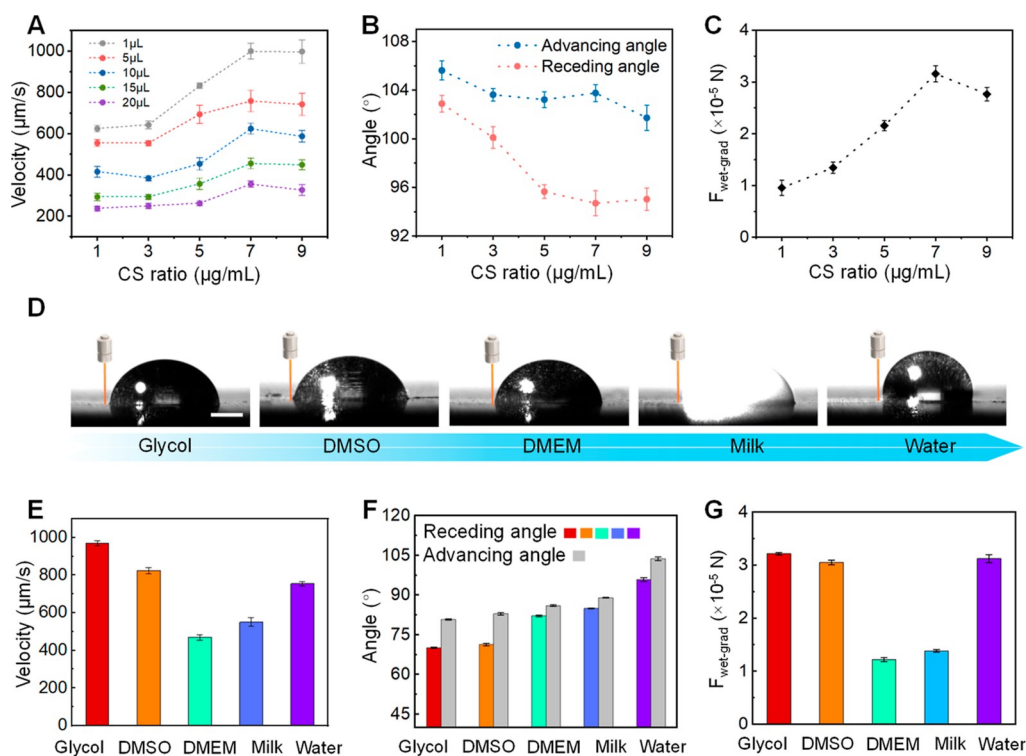
Figure 2. Steering droplets over various CS-LISS recipes. (A) Average sliding velocity of different droplets (1, 5, 10, 15, and 20 μL) with the increase in CS ratio (1, 3, 5, 7, and 9 μg/mL). (B) Advancing/receding angle changes of a water droplet (5 μL) on the CS-LISS with different CS ratios under NIR irradiation. (C) Calculated $F_{wet\text{-}grad}$ for different CS ratios. (D) Images of different types of droplets with different surface tensions on the CS-LISS under unilateral NIR irradiation (CS ratio: 7 μg/mL; scale bar: 1 mm). (E) Average sliding velocity of droplets. (F) Advancing/receding angle changes and (G) $F_{wet\text{-}grad}$ of different types of droplets (5 μL).

characterized in Figure 1B. Here, incomplete combustion of the candle resulted in nanoscale carbon clusters with a single CS particle diameter of approximately 20 nm. The clustering phenomenon of the CS nanoparticles is due to the presence of dangling bonds, which makes the surface of nanoparticles highly reactive.[36,39] The results from high-resolution transmission electron microscopy (HRTEM) and selected area electron diffraction (SAED) confirmed the presence of few pieces of crystalline carbon in the CS along with amorphous carbon [Figure 1C; the diffraction rings observed with SAED are due to (002) and (100) planes of crystalline CS nanoparticles[40]]. The CS contains a high content of carbon (Figure S1) based on the typical element distribution and quantitative energy-dispersive X-ray spectroscopy (EDS) analysis. In addition, the CS also contains a large number of methylene groups and some oxygen-absorbing groups linked to methylene groups (Figure S2), according to the solid-state proton-nuclear magnetic resonance (^{1}H-NMR) of the CS.

Then, the CS nanoparticles were hybridized with polydimethylsiloxane (PDMS) to fabricate a CS-PDMS film. Benefiting from the CS particles, the CS-PDMS film obtained superior photothermal and hydrophobic features. Next, a femtosecond laser was used to cross-scan the CS-PDMS film for texture, as shown in Figure 1D (after cross-scanning, the surface could exhibit superhydrophobic properties and oil storage function); the micropatterns were composed of arrays approximately $160 \times 160 \times 70$ μm in length, width, and height, with the groove width of about 30 μm (Figure S3). After laser ablation, the groove sides of the CS-PDMS film become rough (Figure S4); many particles appear on the surface of the free-laser film, resulting from ablation-caused particle sputtering. In

addition, the CS-PDMS was amorphous, and the laser-texture scanning barely changed the bulk properties of the base CS-PDMS, according to the Fourier transform infrared (FT-IR) spectrum and X-ray diffraction (XRD), as shown in Figures S5 and S6, respectively.

Finally, the CS-LISS was established after dropping the silicone oil lubricant (10 cSt) on the CS-PDMS film (CS-LISS of 5×5 cm is with 10 μL of lubricant). It is noteworthy that although the introduction of the lubricant hardly affects the viability of cells,[9,27] the excess lubricant may wrap around the outside of the water-based droplets and sometimes cause the location offset of droplets after removing the NIR. To prevent over-lubrication, some feasible measures are as follows: the excess lubricant can be removed from the horizontally placed CS-LISS with a thin sheet or be reduced by vertically placing the CS-LISS for 5 min after dropping the lubricant.

Manipulation of Droplets on the CS-LISS with NIR. To show the performance of the CS-LISS, droplets were loaded on the surface, and then, the state of the droplets was switched between sliding and pausing by controlling the on−off of NIR irradiation (Figure 1E and Movie S1). The air/liquid/oil/solid system we developed makes the droplets highly hydrophobic on the surface with a small sliding angle (Figure 1F). The specific droplet driving mechanism is as follows (Figure 1G; γ_{lg}, γ_{og}, and γ_{ol} denote the tensions of liquid−gas, oil−gas, and oil−liquid interfaces, respectively): according to Young's equation $\cos\theta_A = (\gamma_{og} - \gamma_{ol})/\gamma_{lg}$,[41] when NIR irradiates on one side of a droplet, the tension of oil−gas γ_{ol} decreases as the temperature increases, which can significantly increase the advancing angle of the droplet ($\cos\theta_A$); the wetting gradient force ($F_{wet\text{-}grad}$)
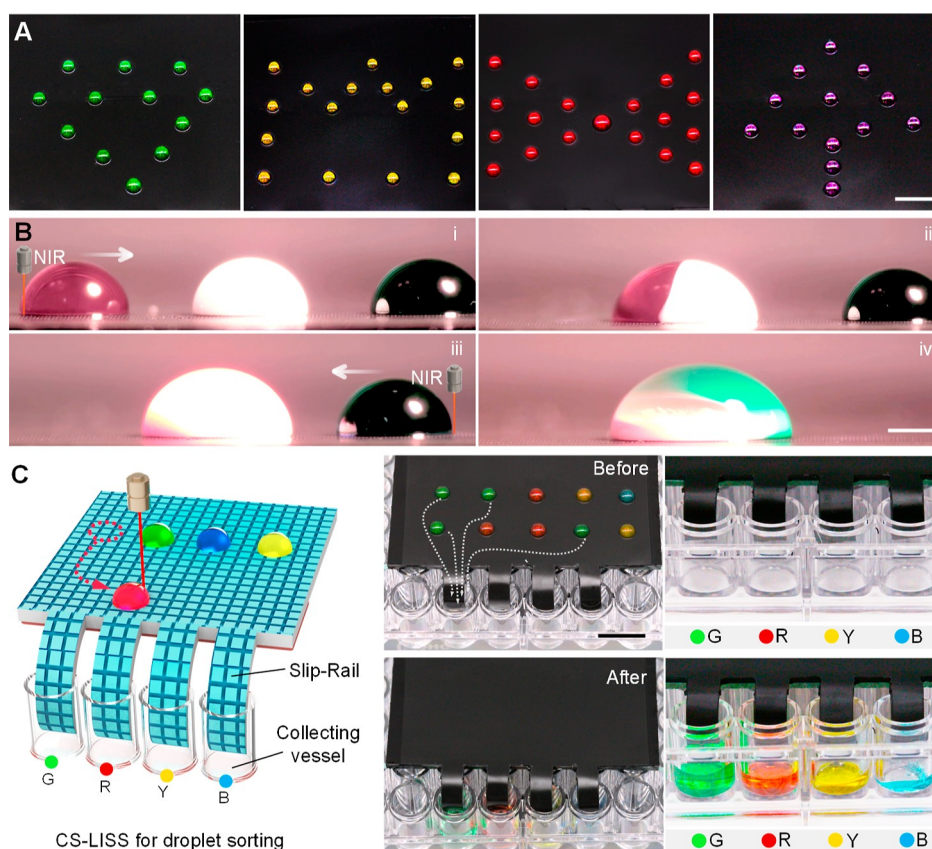
Figure 3. On-demand actuation of diverse droplets along arbitrary routes on the CS-LISS. (A) Programmable patterning with droplets (2 μL; scale bar: 5 mm). (B) Fusion of multiple prodrug droplets (10 μL; scale bar: 2 mm). (C) Schematic and images of the CS-LISS device with a ladder for droplet sorting (5 μL; scale bar: 10 mm).

driving the droplet is manifested as the advancing angle of the droplet is greater than the receding angle, according to the equation $F_{\text{wet-grad}} = \gamma_{\text{lg}}(\cos \theta_{\text{R}} - \cos \theta_{\text{A}}) \times D$[27,42] ($D$ denotes the characteristic length of a droplet on the CS-LISS). Briefly, the maneuvering principle can be assigned to the temperature-difference-induced $F_{\text{wet-grad}}$ resulting in arbitrary sliding routes with the aid of tracing lateral NIR.

Analyses of Factors Affecting the Moving Velocity of Droplets. To make the doped CS-LISS acquire a perfect state and adapt to different prodrug droplet magnitudes, we tested the performance of manipulating droplets with different volumes on the CS-LISS. Here, we chose water droplets for testing because most of the prodrug liquids are water-based. The sliding velocities of droplets with different volumes (1, 5, 10, 15, and 20 μL) under different CS ratios (1, 3, 5, 7, and 9 μg/mL) are shown in Figure 2A. The results show that the droplet velocity on the CS-LISS decreases as the volume increases because of the increase in the mass and adhesion of droplets. The velocity of the droplets increases and then decreases with the CS ratio (the peaks are at 7 μg/mL; the reason for this trend is that when the photothermal nanoparticle content (CS ratio) is low, the photothermal conversion efficiency and then the force increase with the CS ratio; however, when the photothermal nanoparticle content is overly large, the photothermal conversion efficiency decreases, whereas the roughness increases). Considering that $F_{\text{wet-grad}}$ mainly depends on the difference between θ_{A} and θ_{R} of the water-based droplets with the same volume (5 μL; surface tension = 7.2×10^{-2} N/m), we also studied θ_{A} and θ_{R} and the

characteristic length D under different CS ratios. Compared with the water contact angle (WCA) of droplets resting on the CS-LISS (Supporting Information, Figure S7), when NIR irradiation is applied to one side of a droplet, θ_{A} of the droplet increases, whereas θ_{R} decreases. Under different CS ratios (1, 3, 5, 7, and 9 μg/mL), the corresponding $\theta_{\text{A}}/\theta_{\text{R}}$ values were 105.62/102.88, 103.62/100.10, 103.22/95.65, 103.76/94.70, and 101.72/95.03°, respectively (Figure 2B), and the D values were 2.86, 3.11, 3.05, 3.12, and 3.17 mm, respectively (Figure S8A). Based on the equation $F_{\text{wet-grad}} = \gamma_{\text{lg}}(\cos \theta_{\text{R}} - \cos \theta_{\text{A}}) \times D$, $F_{\text{wet-grad}}$ could be calculated as 0.95, 1.35, 2.16, 3.16, and 2.77 ($\times 10^{-5}$ N), respectively (Figure 2C). Specifically, the droplet on the CS-LISS can obtain a maximum wetting gradient force at a ratio of 7 μg/mL.

To apply the CS-LISS for complex prodrug dosing patterns, the maneuverability of the CS-LISS for different droplets was tested. We investigated a series of drops with different surface tensions on the CS-LISS, including glycol, dimethyl sulfoxide (DMSO), Dulbecco's modified Eagle's medium (DMEM), milk, and water (surface tensions of 4.9, 4.3, 5.2, 5.6, and 7.2 ($\times 10^{-2}$) N/m, respectively). The results show that different types of droplets with the same volume (5 μL; Figure 2D) present diverse states (velocity, θ_{A}, θ_{R}, D, and $F_{\text{wet-grad}}$) under NIR irradiation (Figures 2E−G and S8B). Again, the change in $F_{\text{wet-grad}}$ is consistent with the trend of the sliding velocity. Although these types of droplets are manipulated at different velocities due to the difference between θ_{R} and θ_{A}, the CS-
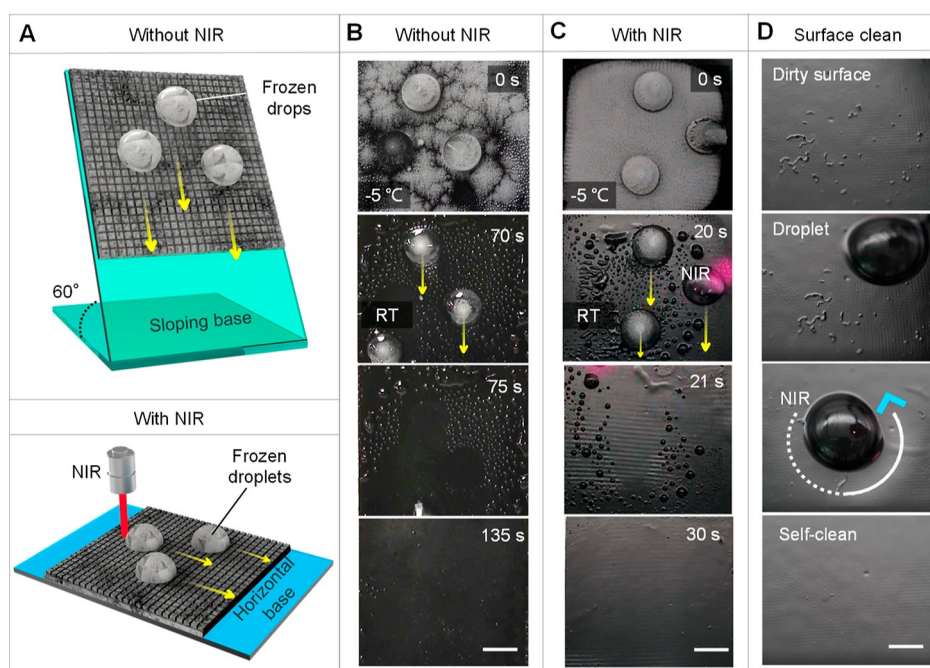
Figure 4. In situ deicing prodrug liquids on the CS-LISS for self-cleaning. (A) Schematic of frozen prodrugs removed from the sloped base passively or from the horizontal base actively by NIR. (B) Images of passive deicing for the CS-LISS. (C) Images of active deicing by NIR for the CS-LISS. (D) Images of the self-cleaning of the CS-LISS via NIR. Scale bar = 10 mm.

LISS is adequately applicable for the manipulation of most water-based drug-laden droplets.

Sorting, Patterning, and Fusion of Droplets on the CS-LISS with NIR. To preliminarily demonstrate the discretionary manipulation capacity of the CS-LISS, a programmable array and fusion of the prodrug droplets (water-based) were performed. As shown in Figure 3A, droplets (2 μL) were maneuvered to the corresponding sites to form the programmable design pattern under NIR irradiation (Figure S9; Movies S2 and S3). Specifically, droplets could reach the target point along any path on the CS-LISS after starting from the inception point. Through multiple NIR manipulations, different kinds of drug droplets can be moved to arbitrary positions and infused with local droplets to form new prodrug droplets (Figure 3B and Movie S4). By regulating the type and volume of droplets, gradient regulation of the mixture concentration can be achieved, which has great significance for drug screening. In addition, we have developed the application of maneuvering ionic conductive droplets (e.g., supersaturated NaCl) on the CS-LISS to control the on−off of a circuit, which may have potential value in the field of microfluidics and electronics (Figure S10).

Microplate technology has been accepted as the most pervasive method for biomedical areas. However, it is time-consuming as a large number of steps are required for pipetting different liquids into all wells.[43] In addition, the pipette needs to be changed frequently for different liquids, which is inefficient and not environmentally friendly (the droplets are easily contaminated). To further exploit the practical values of the CS-LISS, we proposed a strategy for droplet sorting via NIR irradiation. The CS-LISS sorting device consisted of a basal plate and a plurality of slip rails (Figure 3C; Movie S5). A shaped fixation module was glued to the back of the slip rails, ensuring that the rails extended into the collecting vessels. In the presence of NIR irradiation, prodrug droplets on the CS-LISS were sequentially driven along the slip rails to the vessels.

Taking advantage of the hydrophobic properties of the CS-LISS, the droplets exhibited nearly no wastage during the manipulation process, and different types of droplets could smoothly slide into the vessels. Therefore, the CS-LISS-based sorting device, as a noncontact, nondestructive, and efficient transportation platform for droplets, has great application value in biomedicine.

Self-Cleaning Ability of the CS-LISS after Use. In practice, prodrug droplets or hydrogel arrays on a platform are usually exposed to subzero temperatures for cross-linking or preservation.[10,11,15] The traditional method of using glass chips cannot remove the liquid fleetly after freezing, and the chips are often discarded after use due to the liquid residue. Herein, we demonstrate the possibility of the CS-LISS for passive/active deicing and its self-cleaning capability by NIR. As an integrated biological manipulation system, the CS-LISS can effectively remove the residual liquid and be recycled. In the experiments, a series of prodrug droplets were dropped on the CS-LISS and placed in a subzero environment, where the drops quickly froze and a layer of frost formed on the surface. In the passive deicing method, the CS-LISS (5 cm × 5 cm) was placed on a sloping base (Figure 4A) at room temperature (RT). The frost on the surface and at the edge of the frozen droplets starts to thaw after 70 s (Figure 4B). Then, droplets with ice cores will quickly slide off the surface within 5 s. The surface could reach a fresh state in 135 s. When the platform is inconvenient to rotate, the frozen droplets can be actively removed from the horizontal platform with NIR irradiation. Benefiting from the efficient heat transfer performance of the CS-LISS, the edge of frozen droplets thaw very fast (20 s) via NIR irradiation; ice cores can be quickly removed from the surface in 1∼2 s, and it only takes approximately 30 s to reach a fresh surface in the whole process (Figure 4C). During the deicing process, lubricants on the CS-LISS could be consumed, and a lubricant replenishment device may be required in actual scenarios. In addition, the CS-LISS has a convenient self-
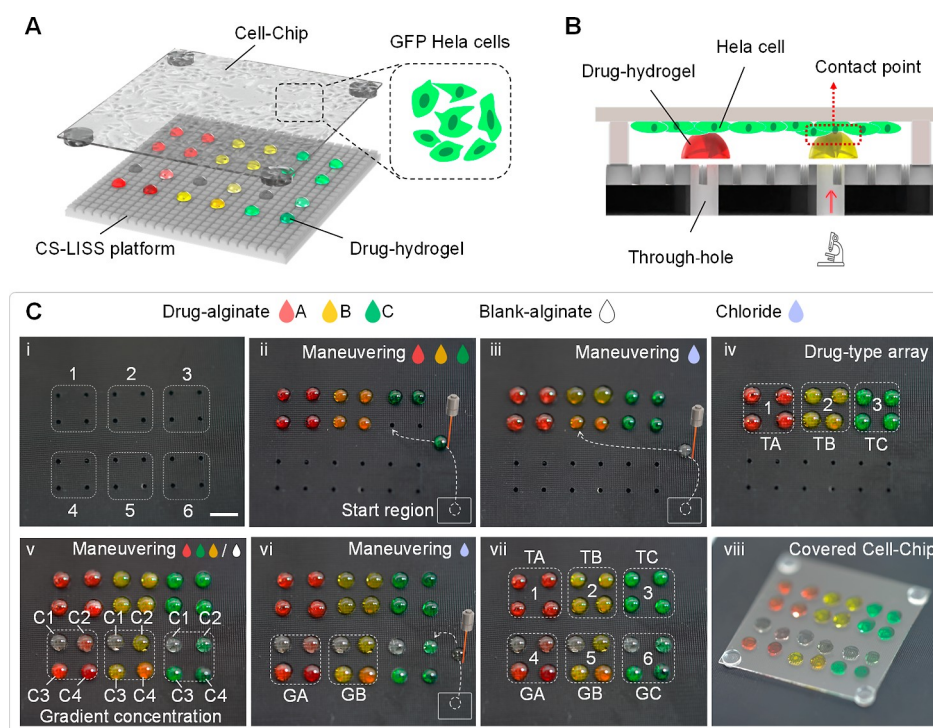
Figure 5. Highly effective manipulation of prodrug droplets for toxicity screening with the CS-LISS. (A) Schematic assembly of the CS-LISS with arrayed prodrug droplets and a cell chip. (B) Cross-sectional view of the toxicity screening system after assembly. (C) Pictures of the formation process of various prodrug-hydrogels on the CS-LISS (scale bar: 3 mm).
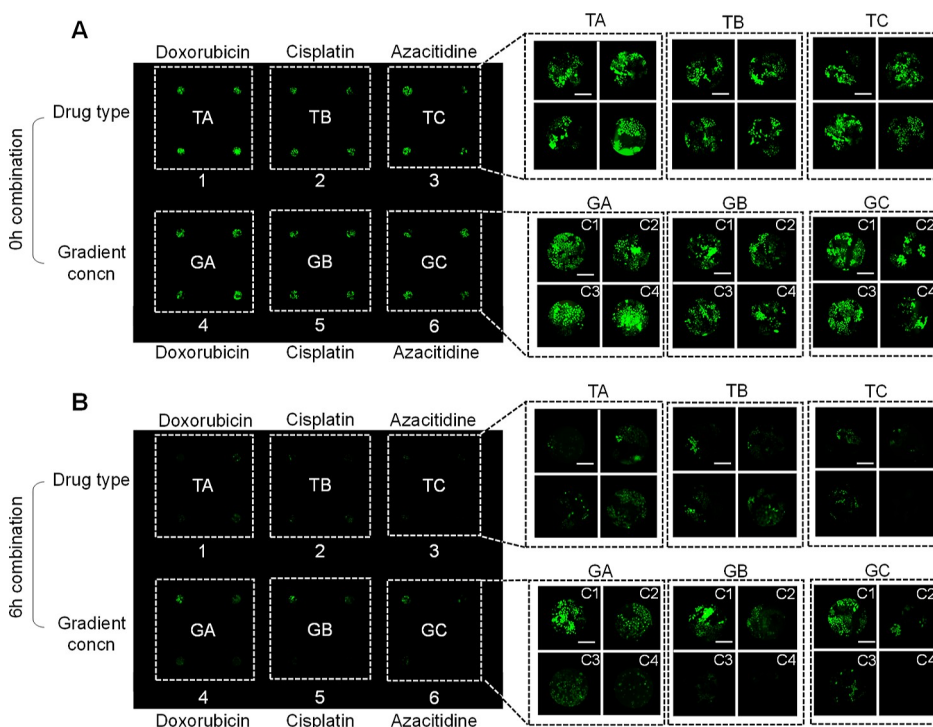

Figure 6. Images of stained HeLa cells in drug toxicity screening with the CS-LISS. (A) Stained cells in the beginning. (B) Stained cells after 6 h. Scale bar: 250 μm.

cleaning capability. Drugs, reagents, and dust left on the surface can be removed by the maneuvered clear water droplets, and then, the platform can be reused (Figure 4D).

High-Throughput Drug Toxicity Screening with the CS-LISS Platform. Taking advantage of the extraordinary mobility, controllable multidroplet fusion capability, and reusability of the CS-LISS, we applied the surface as a drug manipulation platform for high-throughput toxicity screening. Here, different types/concentrations of prodrug-alginate drops were manipulated to specific positions to form a prodrug-hydrogel array (Figure 5A), and then, a cell chip (HeLa cells with a GFP) was covered on top of the array. To facilitate

droplet localization and subsequent fluorescence observation, a series of through-hole arrays on the CS-LISS were carved (Figure 5B). Figure 5C shows the prodrug-hydrogel forming process via NIR manipulation. The CS-LISS was divided into different regions: regions 1, 2, and 3 were for three types of drug-hydrogels (doxorubicin, cisplatin, and azacitidine) with the same concentration, respectively, and regions 4, 5, and 6 were for drug-hydrogels with different concentration gradients. To form drug-hydrogels with the same drug concentration (10 μg/mL), first, three types of drug-alginate droplets (2 μL) were manipulated to each hole in regions 1, 2, and 3; then, 2 μL of calcium chloride droplets were manipulated to the corresponding sites separately for cross-linking to form drug-hydrogel arrays (TA, TB, and TC; Figure 5C(iv)) after 24 h at 4 °C. To form drug-hydrogels with gradient concentrations (0, 5, 10, and 15 μg/mL), different combinations of 1 μL of drug-alginate or blank-alginate were manipulated to the same position three times to form drug-hydrogels with gradient concentrations C1−C4 in regions 4, 5, and 6; then, 1 μL of chloride droplets were manipulated into each site to form gradient drug-hydrogel arrays (GA, GB, and GC; Figure 5C(vi)) after 24 h at 4 °C (the detailed regulation of the drug concentration through plurality solution fusion is shown in Figures S11 and S12). Once the drug-hydrogel arrays were obtained, the cell chip was covered on top (Figure 5C(viii)). The arrays TA, TB, and TC were used to determine whether the drug has an inhibitory effect on the cells, while the arrays GA, GB, and GC were used to determine how the drug affected the viability of cells at different concentrations.

Figure 6 clearly shows the inhibitory effects of various prodrug-hydrogels on HeLa cells. Initially, the cells in all contact points survived well (Figure 6A); after culturing for 6 h at 37 °C, the TA, TB, and TC groups (Figure 6B) showed that almost all HeLa cells were inactivated, verifying the toxicity of the three drugs to the cells. The effects of the above three drugs were observed in the GA, GB, and GC groups, which showed the effects of drug concentration gradients on the cells: in the absence of drugs, after 6 h, the cells remained viable [Figure 6B(C1)]; in the presence of drugs, for all drugs, the viability of cells decreased as the concentration of drugs increased [Figure 6B(C2−C4)]. Specifically, at a concentration of 15 μg/mL [Figure 6B(C4)], doxorubicin, cisplatin, and azacitidine completely killed the HeLa cells. Collectively, high-throughput drug toxicity screening can be achieved on the CS-LISS in terms of both drug-type testing and drug-dose screening.

■ CONCLUSIONS

We fabricated a light-responsive candle-soot-nanoparticle-hybridized lubricant-infused slippery surface (CS-LISS) by one-step femtosecond laser cross-scanning for high-efficiency HTS. Upon the wettability gradient force ($F_{\text{wet-grad}}$) induced by asymmetric NIR, the CS-LISS could readily steer diverse prodrug drops in arbitrary directions to rapidly sort, pattern, and fuse. We investigated the relationship among the CS-doped ratio, droplet wettability variations, $F_{\text{wet-grad}}$, and sliding velocity for diverse liquid species. The droplet on the CS-LISS can obtain a larger wetting gradient force at a ratio of 7 μg/mL, and the CS-LISS can accommodate most water-based prodrug droplet driving operations. In addition, the CS-LISS has the ability to quickly deice, which makes the platform suitable for prodrug removal after cross-linking or preservation. The self-cleaning merit of the CS-LISS allows the platform to be reused

after cleaning. Significantly, we applied the CS-LISS as a toxicity screening platform, and different types/concentrations of drug-hydrogel arrays were formed by multiple NIR manipulations. After the prodrug droplet-laden CS-LISS is combined with a GFP-stained HeLa cell chip, high-efficiency toxicity screening is successfully deployed with the aid of fluorescence imaging. In this article, we briefly demonstrate the feasibility of the CS-LISS as an efficient and flexible prodrug screening platform. Furthermore, the CS-LISS is not limited to manipulating a few drugs. In the future, combined with a quantitative droplet generator and a programmable NIR manipulator, the surface will have broad prospects in microscale HTS.

■ METHODS

Materials. The PDMS Sylgard 184 and silicone oil (10 cSt) were purchased from Dow Corning (Auburn, Ml). CS was collected by placing a glass slide over a candle flame center of about 1 cm. Cyclohexane, glycol, DMSO, and sodium chloride were purchased from Maclin Reagent (Shanghai, China). Sodium alginate, calcium chloride, doxorubicin, cisplatin, and azacitidine were purchased from Aladdin Reagent (Shanghai, China). The chemical structures of the materials mainly added in the droplets for surface testing, cross-linking, and drug testing are provided in Figure S13. HeLa cells with a green fluorescent protein (GFP) were supplied by Procell Life Science & Technology Co., Ltd. (Wuhan, China). DMEM, penicillin−streptomycin (P/S, 1%), trypsin−ethylenediaminetetraacetic acid (0.25%), fetal bovine serum (FBS, 10%), and phosphate-buffered saline were purchased from Thermo Ltd. (Waltham, MA, USA).

Fabrication of the CS-LISS. First, the CS particles were placed into a cyclohexane solution and sonicated for 15 min, and then the PDMS prepolymer was prepared (the ratio of the base material and curing agent was 10:1). Next, the PDMS prepolymer and CS-cyclohexane solution were mechanically mixed for 30 min under 800 rpm stirring. The prepared mixture was poured into a mold and placed in a vacuum chamber for 15 min to remove air bubbles, followed by curing at 65 °C for 12 h. The cured CS/PDMS composite was carefully peeled from the mold. Microgrooves on the CS-PDMS surface were achieved by cross-scanning. The laser beam (104 fs, 1 kHz, 800 nm) from a regenerative amplified Ti: sapphire femtosecond laser system (Legend Elite-1K-HE, Coherent, USA) was employed for ablation. The laser power, scanning spacing, and speed were set at 200 mW, 200 μm, and 1 mm s^{-1}, respectively. Then, the lubricant was injected into the microgrooves of the surface, and the CS-LISS was successfully fabricated.

NIR Light Source. An 808 nm NIR laser (200 mW) was purchased from Standing Laser (Shenzhen, China). The droplets on the CS-LISS surface were maneuvered by NIR irradiation, and the irradiation position of NIR could be adjusted with a mechanical adjustment bracket. In this work, the NIR irradiation distance was set to 10 cm.

Cell Culture. GFP HeLa cells were maintained at 37 °C and 5% CO_2 in basal medium (BM), which consisted of DMEM at 4.5 g/L supplemented with 10% fetal bovine serum (FBS) and 1% penicillin−streptomycin (P/S). HeLa cells were used after the third passage after thawing. To seed the cells onto the cell chip, cells were trypsinized from routine culture and centrifuged at 1200 rpm and 25 °C for 5 min. The supernatant was removed, and the cells were resuspended in fresh culture medium. A hemocytometer was used to count the cells and calculate the seeding density.

Screening Assays for Toxicity. A CS-LISS (5 × 5 cm) was used as the microdrug manipulation platform. Serious hole arrays with a size of 500 μm were drilled in the CS-LISS for droplet positioning and subsequent fluorescence observation. To prevent interference between drugs, the spacing between the holes was larger than 3 mm. The CS-LISS platform was exposed to ultraviolet (UV) light for 2 h before use, and the entire operation process was completed in a biosafety cabinet. First, alginate was mixed in BM to form an alginate-

BM solution (2 mg/mL). Then, drug-alginate is formed by mixing different types of drugs (doxorubicin, cisplatin, and azacitidine) in the alginate-BM solution. For different drug-type experiments, 2 μL of drug-alginate at the same concentration (20 μg/mL) was manipulated into the site by NIR. As the cross-linker, each 2 μL chloride (1 mol/L) droplet was transferred into the site to form drug-hydrogel arrays for 24 h at 4 °C. For different drug concentration experiments, to regulate the drug concentration, we manipulated 1 μL of different combinations of drug-alginate (20 μg/mL) or blank-alginate to the same site three times. Each 1 μL of chloride (1 mol/L) droplet was transferred into the site to form drug-hydrogel arrays. Finally, 4 μL of hydrogels with drug concentrations of 0, 5, 10, and 15 μg/mL were formed at each site after 24 h at 4 °C. For example, a 10 μg/mL drug hydrogel was composed of two drops (2 μL) of drug-alginate, one drop of blank-alginate (1 μL), and one chloride droplet (1 μL, 1 mol/L). The cell chip was made with a 24 × 24 mm glass slip. To create space for hydrogel contact points, four PDMS spacers (diameter of 2 mm amd height of 1 mm) were bonded to the corners of the chip. Before seeding the cells, the cell chip was exposed to UV light for 2 h. HeLa cells were seeded on the cell chip at a density of 3×10^6 cells/mL after culturing for 3 days. The cell chip was covered on the CS-LISS, and it contacted the drug-hydrogel array, which was combined for 6 h at 37 °C.

Characterization. The surface topography of the CS-LISS was investigated by scanning electron microscopy (SEM) (Zeiss EVO 18) after gold sputtering. The structures of the CS were observed by field emission SEM (JSM-2100F, JEOL, Japan) and an optical profiler (XP-1, Ambios, USA). The HRTEM image, SAED pattern, and EDS mapping of CS clusters were observed by field emission SEM (JSM-F200, JEOL, Japan). The chemical nature and phase composition of CS and hybridized materials were analyzed with a nuclear magnetic resonance spectrometer (AV600, Bruker, Switzerland), an infrared spectrometer (Nicolet 8700, Thermo Nicolet, USA), and an X-ray diffractometer (X'Pert MPD, Philips, Holland). The contact angles (CAs) of droplets on samples were measured using an optical CA measuring instrument (Theta Flex, Biolin, Finland) at an ambient temperature. High-magnification movies and optical images for steering diverse droplets were taken using a full-frame camera (Sony A7C, Japan) with a macro lens (Sony SEL9028G, Japan). HeLa cells were imaged using an auto microscope (DMi8, Leica, Germany).

■ ASSOCIATED CONTENT

ⓈⒾ Supporting Information

The Supporting Information is available free of charge at https://pubs.acs.org/doi/10.1021/acsami.2c06973.

> Sliding progress of a water droplet on the CS-LISS via NIR irradiation (MP4),
>
> maneuvering the droplets to form different patterns on the CS-LISS via NIR (MP4),
>
> maneuvering the droplets to form different words on the CS-LISS via NIR (MP4),
>
> multiple droplets fusing on the CS-LISS via NIR (MP4), and
>
> CS-LISS device with a ladder for droplet sorting (MP4) EDS mapping of CS; mapping of C, N, O, and Si elements; EDS spectrums for the atomic percentage of various elements; solid-state ^{1}H nuclear magnetic resonance (NMR) of CS; the optical contour image of the laser textured CS-PDMS surface; the laser textured CS-PDMS imaged with SEM: (A) side views of grooves and (B) top views; FT-IR spectrums for (a) CS, (b) PDMS, (c) CS-PDMS, and (d) laser textured CS-PDMS; XRD spectrums of CS, PDMS, CS-PDMS, and laser textured CS-PDMS; the droplets (5 μL) on the CS-LISS with different CS ratios; images of droplets on the CS-LISS (scale bar: 1 mm); change in the water droplet

> WCA on the CS-LISS; characteristic length of a droplet (5 μL) on the CS-LISS; water droplet with different CS ratios; different types of droplets; programmable words with droplets (scale bar: 5 mm; maneuvering conductive droplets on CS-LISS to selectively turn on the circuit switch (scale bar: 5 mm); schematic illustration of the manipulation strategy for drug type and gradient concentration arrays; the specific formation process of the gradient drug A (doxorubicin); and the chemical structures of the materials mainly added in the droplets for surface testing, cross-linking, and drug testing (PDF)

■ AUTHOR INFORMATION

Corresponding Authors

Li Wen − *Department of Precision Machinery and Instrumentation, University of Science and Technology of China, Hefei 230027, China*; Email: lilywen@ustc.edu.cn

Weiping Ding − *Department of Oncology, the First Affiliated Hospital of USTC, Division of Life Sciences and Medicine, University of Science and Technology of China, Hefei, Anhui 230001, China; Department of Electronic Engineering and Information Science, University of Science and Technology of China, Hefei, Anhui 230027, China*; ⓞ orcid.org/0000-0002-3331-1011; Email: wpdings@ustc.edu.cn

Authors

Shuneng Zhou − *Department of Electronic Engineering and Information Science, University of Science and Technology of China, Hefei, Anhui 230027, China; Department of Oncology, the First Affiliated Hospital of USTC, Division of Life Sciences and Medicine, University of Science and Technology of China, Hefei, Anhui 230001, China*; ⓞ orcid.org/0000-0003-3710-9264

Chao Chen − *Department of Materials Physics and New Energy Device, School of Materials Science and Engineering, Hefei University of Technology, Hefei 230009, China*; ⓞ orcid.org/0000-0002-8061-0292

Junfeng Yang − *Department of Precision Machinery and Instrumentation, University of Science and Technology of China, Hefei 230027, China*

Lirui Liao − *Department of Precision Machinery and Instrumentation, University of Science and Technology of China, Hefei 230027, China*

Zekun Wang − *Department of Precision Machinery and Instrumentation, University of Science and Technology of China, Hefei 230027, China*

Dong Wu − *Department of Precision Machinery and Instrumentation, University of Science and Technology of China, Hefei 230027, China*; ⓞ orcid.org/0000-0003-0623-1515

Jiaru Chu − *Department of Precision Machinery and Instrumentation, University of Science and Technology of China, Hefei 230027, China*; ⓞ orcid.org/0000-0001-6472-8103

Complete contact information is available at: https://pubs.acs.org/10.1021/acsami.2c06973

Author Contributions

S.Z. and C.C. contribute equally. S.Z. and C.C. conceived the idea; S.Z. carried out experiments including device fabrication and performance characterization with the help of J.Y. and Z.K; L.L. performed the sliding velocity measurement of

droplets; D.W. and J.C. discussed the results and commented on the article. W.D., L.W., and C.C. edited, review, and discussed the results. All authors accepted the final version of the article.

Notes

■ ACKNOWLEDGMENTS

■ REFERENCES

(1) Baillie, T. A. Future of toxicology-metabolic activation and drug design: Challenges and opportunities in chemical toxicology. *Chem. Res. Toxicol.* **2006**, *19*, 889−893.

(2) Petricoin, E. F.; Zoon, K. C.; Kohn, E. C.; Barrett, J. C.; Liotta, L. A. Clinical proteomics: Translating benchside promise into bedside reality. *Nat. Rev. Drug Discov.* **2002**, *1*, 683−695.

(3) Dunn, D. A.; Feygin, I. Challenges and solutions to ultra-high-throughput screening assay miniaturization: submicroliter fluid handling. *Drug Discov. Today* **2000**, *5*, S84−S91.

(4) Kasibhatla, S.; Gourdeau, H.; Meerovitch, K.; Drewe, J.; Reddy, S.; Qiu, L.; Zhang, H.; Bergeron, F.; Bouffard, D.; Yang, Q.; et al. Discovery and mechanism of action of a novel series of apoptosis inducers with potential vascular targeting activity. *Mol. Cancer Ther.* **2004**, *3*, 1365−1374.

(5) Mueller, H.; Kassack, M. U.; Wiese, M. Comparison of the usefulness of the MTT, ATP, and calcein assays to predict the potency of cytotoxic agents in various human cancer cell lines. *J. Biomol. Screen* **2004**, *9*, 506−515.

(6) Bailey, S. N.; Sabatini, D. M.; Stockwell, B. R. Microarrays of small molecules embedded in biodegradable polymers for use in mammalian cell-based screens. *Proc. Natl. Acad. Sci. USA* **2004**, *101*, 16144−16149.

(7) Moroni, L.; Burdick, J. A.; Highley, C.; Lee, S. J.; Morimoto, Y.; Takeuchi, S.; Yoo, J. J. Biofabrication strategies for 3D in vitro models and regenerative medicine. *Nat. Rev. Mater.* **2018**, *3*, 21−37.

(8) Rodrigues, A. L.; Diogo, M. M.; Cabral, J. M. S.; Dordick, J. S. Advanced microtechnologies for high-throughput screening. *Eng. Strategies Regener. Med.* **2020**, 149−175.

(9) Ganguli, A.; Mostafa, A.; Saavedra, C.; Kim, Y.; Le, P.; Faramarzi, V.; Feathers, R. W.; Berger, J.; Ramos-Cruz, K. P.; Adeniba, O.; et al. Three-dimensional microscale hanging drop arrays with geometric control for drug screening and live tissue imaging. *Sci. Adv.* **2021**, *7*, No. eabc1323.

(10) Lee, M.-Y.; Park, C. B.; Dordick, J. S.; Clark, D. S. Metabolizing enzyme toxicology assay chip (MetaChip) for high-throughput microscale toxicity analyses. *Proc. Natl. Acad. Sci. USA* **2005**, *102*, 983−987.

(11) Lee, M.-Y.; Kumar, R. A.; Sukumaran, S. M.; Hogg, M. G.; Clark, D. S.; Dordick, J. S. Three-dimensional cellular microarray for high-throughput toxicology assays. *Proc. Natl. Acad. Sci. USA* **2008**, *105*, 59−63.

(12) Yi, H.-G.; Kim, H.; Kwon, J.; Choi, Y.-J.; Jang, J.; Cho, D.-W. Application of 3D bioprinting in the prevention and the therapy for human diseases. *Signal Transduct. Targeted Ther.* **2021**, *6*, 177.

(13) Ueda, E.; Levkin, P. A. Emerging Applications of Super-hydrophilic-Superhydrophobic Micropatterns. *Adv. Mater.* **2013**, *25*, 1234−1247.

(14) Li, Y.; Chen, P.; Wang, Y.; Yan, S.; Feng, X.; Du, W.; Koehler, S. A.; Demirci, U.; Liu, B.-F. Rapid Assembly of Heterogeneous 3D Cell Microenvironments in a Microgel Array. *Adv. Mater.* **2016**, *28*, 3543−3548.

(15) Neto, A. I.; Demir, K.; Popova, A. A.; Oliveira, M. B.; Mano, J. F.; Levkin, P. A. Fabrication of Hydrogel Particles of Defined Shapes Using Superhydrophobic-Hydrophilic Micropatterns. *Adv. Mater.* **2016**, *28*, 7613−7619.

(16) Bang, H.; Lim, S. H.; Lee, Y. K.; Chung, S.; Chung, C.; Han, D.-C.; Chang, J. K. Serial dilution microchip for cytotoxicity test. *J. Micromech. Microeng.* **2004**, *14*, 1165−1170.

(17) Yang, Z.; Wei, J.; Sobolev, Y. I.; Grzybowski, B. A. Systems of mechanized and reactive droplets powered by multi-responsive surfactants (vol 553, pg 313, 2018). *Nature* **2019**, *567*, No. E11.

(18) Wu, Y.; Feng, J.; Gao, H.; Feng, X.; Jiang, L. Superwettability-Based Interfacial Chemical Reactions. *Adv. Mater.* **2019**, *31*, 1800718.

(19) Tang, X.; Zhu, P.; Tian, Y.; Zhou, X.; Kong, T.; Wang, L. Mechano-regulated surface for manipulating liquid droplets. *Nat. Commun.* **2017**, *8*, 14831.

(20) Song, Y.; Michaels, T. C. T.; Ma, Q.; Liu, Z.; Yuan, H.; Takayama, S.; Knowles, T. P. J.; Shum, H. C. Budding-like division of all-aqueous emulsion droplets modulated by networks of protein nanofibrils. *Nat. Commun.* **2018**, *9*, 2110.

(21) Huang, Z.; Su, M.; Yang, Q.; Li, Z.; Chen, S.; Li, Y.; Zhou, X.; Li, F.; Song, Y. A general patterning approach by manipulating the evolution of two-dimensional liquid foams. *Nat. Commun.* **2017**, *8*, 14110.

(22) Sun, Q.; Wang, D.; Li, Y.; Zhang, J.; Ye, S.; Cui, J.; Chen, L.; Wang, Z.; Butt, H.-J.; Vollmer, D.; et al. Surface charge printing for programmed droplet transport. *Nat. Mater.* **2019**, *18*, 936−941.

(23) Jung, J. H.; Destgeer, G.; Ha, B.; Park, J.; Sung, H. J. On-demand droplet splitting using surface acoustic waves. *Lab Chip* **2016**, *16*, 3235−3243.

(24) Huang, G.; Li, M.; Yang, Q.; Li, Y.; Liu, H.; Yang, H.; Xu, F. Magnetically Actuated Droplet Manipulation and Its Potential Biomedical Applications. *ACS Appl. Mater. Interfaces* **2017**, *9*, 1155−1166.

(25) Qi, L.; Niu, Y.; Ruck, C.; Zhao, Y. Mechanical-activated digital microfluidics with gradient surface wettability. *Lab Chip* **2019**, *19*, 223−232.

(26) Lv, J.-a.; Liu, Y.; Wei, J.; Chen, E.; Qin, L.; Yu, Y. Photocontrol of fluid slugs in liquid crystal polymer microactuators. *Nature* **2016**, *537*, 179−184.

(27) Wu, S.; Zhou, L.; Chen, C.; Shi, L.-A.; Zhu, S.; Zhang, C.; Meng, D.; Huang, Z.; Li, J.; Hu, Y.; et al. Photothermal Actuation of Diverse Liquids on an Fe3O4-Doped Slippery Surface for Electric Switching and Cell Culture. *Langmuir* **2019**, *35*, 13915−13922.

(28) Ichimura, K.; Oh, S.-K.; Nakagawa, M. Light-driven motion of liquids on a photoresponsive surface. *Science* **2000**, *288*, 1624−1626.

(29) Chen, C.; Huang, Z.; Shi, L. A.; Jiao, Y.; Zhu, S.; Li, J.; Hu, Y.; Chu, J.; Wu, D.; Jiang, L. Remote Photothermal Actuation of Underwater Bubble toward Arbitrary Direction on Planar Slippery Fe3O4-Doped Surfaces. *Adv. Funct. Mater.* **2019**, *29*, 1904766.

(30) Kwon, G.; Panchanathan, D.; Mahmoudi, S. R.; Gondal, M. A.; McKinley, G. H.; Varanasi, K. K. Visible light guided manipulation of liquid wettability on photoresponsive surfaces. *Abstr. Pap. Am. Chem. Soc.* **2017**, *8*, 14968.

(31) Wu, S.; Du, Y.; Alsaid, Y.; Wu, D.; Hua, M.; Yan, Y.; Yao, B.; Ma, Y.; Zhu, X.; He, X. Superhydrophobic photothermal icephobic surfaces based on candle soot. *Proc. Natl. Acad. Sci. USA* **2020**, *117*, 11240−11246.

(32) Yin, X.; Zhang, Y.; Wang, D.; Liu, Z.; Liu, Y.; Pei, X.; Yu, B.; Zhou, F. Integration of Self-Lubrication and Near-Infrared Photo-thermogenesis for Excellent Anti-Icing/Deicing Performance. *Adv. Funct. Mater.* **2015**, *25*, 4237−4245.

(33) Cheng, T.; He, R.; Zhang, Q.; Zhan, X.; Chen, F. Magnetic particle-based super-hydrophobic coatings with excellent anti-icing and thermoresponsive deicing performance. *J. Mater. Chem. A* **2015**, *3*, 21637−21646.

(34) Iqbal, R.; Majhy, B.; Sen, A. K. Facile Fabrication and Characterization of a PDMS-Derived Candle Soot Coated Stable Biocompatible Superhydrophobic and Superhemophobic Surface. *ACS Appl. Mater. Interfaces* **2017**, *9*, 31170−31180.

(35) Zhang, B.; Duan, J.; Huang, Y.; Hou, B. Double layered superhydrophobic PDMS-Candle soot coating with durable corrosion resistance and thermal-mechanical robustness. *J. Mater. Sci. Technol.* **2021**, *71*, 1−11.

(36) Sahoo, B. N.; Kandasubramanian, B. An experimental design for the investigation of water repellent property of candle soot particles. *Mater. Chem. Phys.* **2014**, *148*, 134−142.

(37) Deng, X.; Mammen, L.; Butt, H.-J.; Vollmer, D. Candle Soot as a Template for a Transparent Robust Superamphiphobic Coating. *Science* **2012**, *335*, 67−70.

(38) Sun, W.; Zhang, X.; Jia, H. R.; Zhu, Y. X.; Guo, Y.; Gao, G.; Li, Y. H.; Wu, F. G. Water-Dispersible Candle Soot-Derived Carbon Nano-Onion Clusters for Imaging-Guided Photothermal Cancer Therapy. *Small* **2019**, *15*, 1804575.

(39) Seo, K.; Kim, M.; Kim, D. H. Candle-based process for creating a stable superhydrophobic surface. *Carbon* **2014**, *68*, 583−596.

(40) Ghosh, T.; Ghosh, R.; Basak, U.; Majumdar, S.; Ball, R.; Mandal, D.; Nandi, A. K.; Chatterjee, D. P. Candle soot derived carbon nanodot/polyaniline hybrid materials through controlled grafting of polyaniline chains for supercapacitors. *J. Mater. Chem. A* **2018**, *6*, 6476−6492.

(41) Good, R. J. Thermodynamic Derivation of Wenzels Modification of Youngs Equation for Contact Angles - Together with a Theory of Hysteresis. *J. Am. Chem. Soc.* **1952**, *74*, 5041−5042.

(42) Chaudhury, M. K.; Whitesides, G. M. How to Make Water Run Uphill. *Science* **1992**, *256*, 1539−1541.

(43) Wang, J.; Sun, L.; Zou, M.; Gao, W.; Liu, C.; Shang, L.; Gu, Z.; Zhao, Y. Bioinspired shape-memory graphene film with tunable wettability. *Sci. Adv.* **2017**, *3*, 1700004.